Quantifying Balance Capabilities using Momentum Gain

Brandon J DeHart and Dana Kulić

Abstract— **The ability of a legged system to balance depends on both the control strategy used and the system's physical design. To quantify a system's inherent balance capabilities, we define momentum gains for general 2D and 3D models. We provide two methods for calculating these gains, and relate both velocity and momentum gains to the centroidal momentum of a system, a commonly used measure of aggregate system behavior. Finally, we compare velocity and momentum gains as criteria for the design of simple balancing systems using a parameterized optimization framework.**

I. Introduction

Balance is a critical capability for a wide variety of robots and other mechatronic systems. Any time there is a small area contact with the environment which includes ground reaction force transmission, some degree of active balance is required. A variety of balancing control algorithms have been proposed [1]–[5]; In particular, many existing balance controllers regulate centroidal momentum (e.g., [2]–[4]).

Less work has focused on how to quantify a mechanism's inherent balancing capabilities, or how to modify the mechanism to improve these capabilities. Recently, Azad *et al.* proposed a formulation of the dynamic Center of Mass (COM) manipulability [6], which defines an ellipsoid in 3D space that outlines the system's physical COM acceleration limits. However, this metric depends on the specification of a weighting matrix for normalization and the ellipsoid must be projected into lower dimensions to be used for balance.

Featherstone developed dynamic ratios called *velocity gains* [7], which quantify how fast an articulating system balancing on a passive contact can move its COM. Velocity gains are independent of the controller used, as they are functions of the physical properties of the mechanism, and define a limit on how well any controller could balance the mechanism[1]. These gains were recently used in the development of effective planar balance controllers [8]–[10].

Velocity gains are invariant to a scaling of the system's total mass, and the angular velocity gain is also invariant to a scaling of length, allowing the balance abilities of an entire class of mechanisms to be quantified with one metric [7]. Featherstone also defined scalar *momentum gains* for a planar 2-link inverted pendulum.

In this paper, we introduce notation which simplifies the gain equations and then build on Featherstone's work to:

- Extend momentum gain to general 2D and 3D models;
- Define two methods for calculating momentum gains for these general 2D and 3D models; and
- Relate the definitions of velocity and momentum gains to the system's centroidal momentum.

These momentum gains inherit the corresponding velocity gains' independence from the applied control scheme and invariance properties, in addition to including a consideration of the inertial properties of the system. These properties make the momentum gains a good choice for analyzing the balance capabilities of a given mechanism, or as a criterion for optimizing the design of balancing mechanisms.

II. Velocity Gain: Review

Linear velocity gain [7] is defined as a ratio of the change in horizontal COM velocity relative to an impulsive change in the velocity of the model's actuated joint(s), assuming a single passive (rolling or point) contact with the environment.

Similarly, angular velocity gain [7] is defined as a ratio of the change in angular COM velocity about the (instantaneous, if rolling) contact point relative to an impulsive change in the velocity of the model's actuated joint(s).

For 3D models, the linear velocity gain $\boldsymbol{G}_v$ includes both horizontal directions of motion, while the angular velocity gain $\boldsymbol{G}_\omega$ includes all 3 rotations[2] about the contact point:

$$\boldsymbol{G}_v(\Delta\dot{\boldsymbol{q}}_a) = \begin{bmatrix}\Delta\dot{c}_x \\ \Delta\dot{c}_y\end{bmatrix} \quad \boldsymbol{G}_\omega(\Delta\dot{\boldsymbol{q}}_a) = \Delta\dot{\boldsymbol{\phi}} = \frac{\boldsymbol{c}\times\Delta\dot{\boldsymbol{c}}}{c^2} \quad (1)$$

where $\boldsymbol{c} = [c_x\ c_y\ c_z]^T$ is a vector from the contact point to the COM (see Figure 1a) with length $c = ||\boldsymbol{c}||_2$, the change in COM velocity is $\Delta\dot{\boldsymbol{c}} = [\Delta\dot{c}_x\ \Delta\dot{c}_y\ \Delta\dot{c}_z]^T$, the change in angular COM velocity about the contact point is $\Delta\dot{\boldsymbol{\phi}} = [\Delta\dot{\phi}_x\ \Delta\dot{\phi}_y\ \Delta\dot{\phi}_z]^T$, and the change in actuated joint velocity is $\Delta\dot{\boldsymbol{q}}_a$. Note that in these equations, it is assumed that $\Delta\dot{\boldsymbol{q}}_a$ is a unit velocity step (i.e., $||\Delta\dot{\boldsymbol{q}}_a|| = 1$) [7]. Both gains are divided by the velocity step magnitude, which gives $\boldsymbol{G}_v$ units of length and makes $\boldsymbol{G}_\omega$ dimensionless.

For a planar model, we assume that gravity acts in the $-\mathbf{y}$ direction and set $c_z = 0$, resulting in $\boldsymbol{\phi} = [0\ 0\ \phi_z]^T$ (see Figure 1b). Using this to simplify Equation (1), we can extract the scalar velocity gains defined in [7] for planar models: $G_v(\Delta\dot{\boldsymbol{q}}_a) = \Delta\dot{c}_x$ and $G_\omega(\Delta\dot{\boldsymbol{q}}_a) = \Delta\dot{\phi}_z$.

Three methods of calculating the velocity gains are given in [7]: Direct, COM Jacobian, and Augmented Inertia Matrix.

*This work was supported by the Natural Sciences and Engineering Research Council of Canada (NSERC).

Brandon J DeHart and Dana Kulić are with the Department of Electrical & Computer Engineering, University of Waterloo, Ontario, Canada.
{bjdehart,dana.kulic}@uwaterloo.ca

[1]In this context, balance is assumed to be primarily a function of COM motion. Angular momentum about the COM is assumed to be regulated.

[2]Although the $\boldsymbol{G}_\omega$ component about the vertical axis does not contribute to balance, it was included in the original definition of $\boldsymbol{G}_\omega$ along with a brief discussion of how it could be used in spinning motions [7].

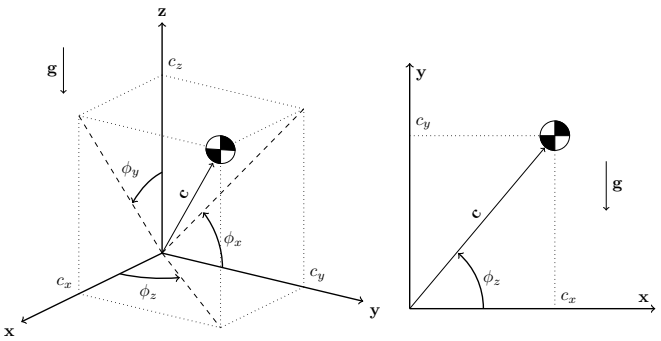

(a) 3D Coordinates (b) 2D Coordinates

Fig. 1. In general, $\boldsymbol{c} = [c_x\ c_y\ c_z]^T$ is a vector from the contact point to the COM and the angles $\boldsymbol{\phi} = [\phi_x\ \phi_y\ \phi_z]^T$ are measured from the reference frame to $\boldsymbol{c}$. For 2D, we assume gravity acts in the $-\mathbf{y}$ direction and $c_z = 0$.

In the Augmented Inertia Matrix method, virtual immobile prismatic joints (labeled $0 = \{x, y, z\}$) are inserted between the passive contact and the inertial reference frame.

The impulsive equations, with 3 virtual prismatic joints (labeled 0) and 3 passive rotational joints (labeled p) at the contact and the actuated joints (labeled a), are therefore:

$$\boldsymbol{H}'\Delta\dot{\boldsymbol{q}}' = \begin{bmatrix} \boldsymbol{H}_{00} & \boldsymbol{H}_{0p} & \boldsymbol{H}_{0a} \\ \boldsymbol{H}_{p0} & \boldsymbol{H}_{pp} & \boldsymbol{H}_{pa} \\ \boldsymbol{H}_{a0} & \boldsymbol{H}_{ap} & \boldsymbol{H}_{aa} \end{bmatrix} \begin{bmatrix} 0 \\ \Delta\dot{\boldsymbol{q}}_p \\ \Delta\dot{\boldsymbol{q}}_a \end{bmatrix} = \begin{bmatrix} \boldsymbol{\iota}_0 \\ 0 \\ \boldsymbol{\iota}_a \end{bmatrix} \quad (2)$$

where $\boldsymbol{\iota}_0$ and $\boldsymbol{\iota}_a$ are virtual joint and actuated joint impulses, respectively, and $\boldsymbol{H}'$ is the Augmented Joint Space Inertia Matrix[3]. This enables the direct calculation of $\Delta\dot{\boldsymbol{c}}$ since the virtual impulse $\boldsymbol{\iota}_0 = m\Delta\dot{\boldsymbol{c}}$, where m is the total mass [7].

Since $\boldsymbol{H}_{pp}$ is a 3x3 symmetric positive definite matrix, we can use the middle row to get $\Delta\dot{\boldsymbol{q}}_p = -\boldsymbol{H}_{pp}^{-1}\boldsymbol{H}_{pa}\Delta\dot{\boldsymbol{q}}_a$ as discussed in [7], and the equation for $\Delta\dot{\boldsymbol{c}}$ becomes:

$$\Delta\dot{\boldsymbol{c}} = \frac{1}{m}\left(\boldsymbol{H}_{0a} - \boldsymbol{H}_{0p}\boldsymbol{H}_{pp}^{-1}\boldsymbol{H}_{pa}\right)\Delta\dot{\boldsymbol{q}}_a = \frac{1}{m}\bar{\boldsymbol{H}}_{0a}\Delta\dot{\boldsymbol{q}}_a \quad (3)$$

To simplify this equation, we introduce the notation $\bar{\boldsymbol{H}}$ to denote the relationship between impulse and a change in actuated joint velocities (i.e., $\boldsymbol{\iota}_0 = \bar{\boldsymbol{H}}_{0a}\Delta\dot{\boldsymbol{q}}_a$). In general, this notation can be written as follows:

$$\bar{\boldsymbol{H}}_{\beta\alpha} = \boldsymbol{H}_{\beta\alpha} - \boldsymbol{H}_{\beta p}\boldsymbol{H}_{pp}^{-1}\boldsymbol{H}_{p\alpha} \quad (4)$$

where both α and the β can be either a single joint index or a range of indices provided $\alpha \subset a$. In 2D, with only one passive rotational contact joint ($p = \{1\}$): $\boldsymbol{H}_{pp}^{-1} = 1/H_{11}$.

In any given configuration, the matrix $\boldsymbol{H}'$ and vector $\boldsymbol{c}$ are fixed. Since the velocity gain equations are linear with respect to $\Delta\dot{\boldsymbol{q}}_a$, we define gain matrices $\boldsymbol{G}_{*a}$ such that $\boldsymbol{G}_v(\Delta\dot{\boldsymbol{q}}_a) = \boldsymbol{G}_{va}\Delta\dot{\boldsymbol{q}}_a$ and $\boldsymbol{G}_\omega(\Delta\dot{\boldsymbol{q}}_a) = \boldsymbol{G}_{\omega a}\Delta\dot{\boldsymbol{q}}_a$ [7].

Using the new notation above, these gain matrices are:

$$\boldsymbol{G}_{va} = \frac{1}{m}\begin{bmatrix} \bar{\boldsymbol{H}}_{xa} \\ \bar{\boldsymbol{H}}_{ya} \end{bmatrix} \qquad \boldsymbol{G}_{\omega a} = \frac{1}{mc^2}[\boldsymbol{c}\times]\bar{\boldsymbol{H}}_{0a} \quad (5)$$

[3]The standard Joint Space Inertia Matrix $\boldsymbol{H}$ is simply the submatrix of $\boldsymbol{H}'$ where all elements with a 0 in the subscript have been removed.

where $[\boldsymbol{c}\times]$ represents the 3x3 skew symmetric matrix.

For 2D systems, the (horizontal) gain vectors from [7] can be extracted from these general gain matrices: the first row of $\boldsymbol{G}_{va}$ is the linear velocity gain vector, and the third (last) row of $\boldsymbol{G}_{\omega a}$ is the angular gain vector.

Since the only restriction on $\Delta\dot{\boldsymbol{q}}_a$ is that $||\Delta\dot{\boldsymbol{q}}_a|| = 1$, the relative values of its elements can be selected to achieve a given system behavior. As an example, if only one specific joint is to be used for balance, then the $\Delta\dot{\boldsymbol{q}}_a$ element for that joint can be set to 1 and all other elements can be set to 0.

A. 2-Link Planar Momentum Gain

A 2-link planar inverted pendulum, the simplest balancing mechanism, has only one actuated joint ($a = \{2\}$) so its scalar velocity gains can be directly defined as ratios [7]:

$$G_v = \frac{\Delta\dot{c}_x}{\Delta\dot{q}_2} \qquad G_\omega = \frac{\Delta\dot{\phi}_z}{\Delta\dot{q}_2} \quad (6)$$

Building on these definitions, Featherstone also defined scalar momentum gains for the 2-link planar model [7]:

- Linear momentum gain (G_m), defined as a measure of the change in horizontal linear COM momentum due to an impulse at the actuated joint:

$$G_m = \frac{m\Delta\dot{c}_x}{\iota_2} = mG_v\frac{\Delta\dot{q}_2}{\iota_2} \quad (7)$$

- Angular momentum gain (G_o), defined as a measure of the change in the moment of momentum of the COM about the contact due to an impulse at the actuated joint:

$$G_o = \frac{mc^2\Delta\dot{\phi}_z}{\iota_2} = mc^2G_\omega\frac{\Delta\dot{q}_2}{\iota_2} \quad (8)$$

Note that G_o is defined using the change in the moment of momentum about the contact (effectively, the angular momentum about the contact due to COM motion). This is not the change in total angular momentum about the contact, which is always 0 for a passive rotary joint [7].

As shown above, momentum gains are directly related to velocity gains. For the 2-link planar model, they are both strictly positive multiples of their respective velocity gains, since $\boldsymbol{H}$ is positive definite and $\Delta\dot{q}_2/\iota_2 = H_{11}/\det(\boldsymbol{H})$ [7]. In light of this, Featherstone concluded that there was no objective reason to use momentum gains.

III. Momentum Gain

In this section, we expand the initial definition of momentum gain above to general models in 2D and 3D, and introduce an augmented inertia method for calculating these general momentum gains. Another method for calculating both velocity and momentum gains is introduced using *spatial notation* (see [11], [12]). This spatial method for calculating gains depends on the direct relationship between a system's gains and its *centroidal momentum* [3], [13].

The linear momentum gain $\boldsymbol{G}_m$ and the angular momentum gain $\boldsymbol{G}_o$ for a general system are defined (using the change in linear COM momentum $\Delta\boldsymbol{l} = \boldsymbol{\iota}_0 = m\Delta\dot{\boldsymbol{c}}$) as:

$$\boldsymbol{G}_m(\boldsymbol{\iota}_a) = \begin{bmatrix} \Delta l_x \\ \Delta l_y \end{bmatrix} \quad \boldsymbol{G}_o(\boldsymbol{\iota}_a) = mc^2\Delta\dot{\boldsymbol{\phi}} = \boldsymbol{c}\times\Delta\boldsymbol{l} \quad (9)$$

Note that the actuator impulse vector $\boldsymbol{\iota}_a$ in these equations is now assumed to be a unit step impulse ($||\boldsymbol{\iota}_a|| = 1$), similar to the unit velocity step assumption on $\Delta\dot{\boldsymbol{q}}_a$ used in Equation (1). Dividing the gains by the step impulse magnitude gives $\boldsymbol{G}_m$ units of reciprocal length and makes $\boldsymbol{G}_o$ dimensionless.

There are two key differences between the momentum gain equations in (9) and the velocity gain equations in (1). First, the angular momentum gain equation does not include the division by c^2 which is present in the angular velocity gain. This means that angular momentum gain is always finite, while the angular velocity gain approaches infinity as c approaches 0 and is undefined at $c = 0$.

Second, these equations now assume a unit step impulse instead of a unit velocity step, which inherently incorporates inertial information into the momentum gain. As shown in the next section, this inertial information enables the momentum gain to act as a measurement of how quickly the model can move its COM for unit motor impulses. In effect, a higher momentum gain implies less motor effort (i.e., less power) is required to achieve the same COM movement.

A. Augmented Inertia Method

Recall that we can use our augmented inertia notation to show that $\boldsymbol{\iota}_a = \bar{\boldsymbol{H}}_{aa}\Delta\dot{\boldsymbol{q}}_a$. Using the matrix determinant lemma, we can show that $\bar{\boldsymbol{H}}_{aa} = \boldsymbol{H}_{aa} - \boldsymbol{H}_{ap}\boldsymbol{H}_{pp}^{-1}\boldsymbol{H}_{pa}$ is invertible. This can then be used to solve for $\Delta\dot{\boldsymbol{q}}_a$ given an actuator impulse unit vector: $\Delta\dot{\boldsymbol{q}}_a = \bar{\boldsymbol{H}}_{aa}^{-1}\boldsymbol{\iota}_a$.

We can now define an equation for $\Delta\boldsymbol{l}$ in terms of $\boldsymbol{\iota}_a$:

$$\Delta\boldsymbol{l} = \boldsymbol{\iota}_0 = \bar{\boldsymbol{H}}_{0a}\Delta\dot{\boldsymbol{q}}_a = \bar{\boldsymbol{H}}_{0a}\bar{\boldsymbol{H}}_{aa}^{-1}\boldsymbol{\iota}_a \tag{10}$$

This also allows us to define the momentum gain matrices $\boldsymbol{G}_{ma}$ and $\boldsymbol{G}_{oa}$ in terms of the velocity gain matrices, where $\boldsymbol{G}_m(\boldsymbol{\iota}_a) = \boldsymbol{G}_{ma}\boldsymbol{\iota}_a$ and $\boldsymbol{G}_o(\boldsymbol{\iota}_a) = \boldsymbol{G}_{oa}\boldsymbol{\iota}_a$, as:

$$\boldsymbol{G}_{ma} = \begin{bmatrix}\bar{\boldsymbol{H}}_{xa}\\ \bar{\boldsymbol{H}}_{ya}\end{bmatrix}\bar{\boldsymbol{H}}_{aa}^{-1} = m\boldsymbol{G}_{va}\bar{\boldsymbol{H}}_{aa}^{-1} \tag{11}$$

$$\boldsymbol{G}_{oa} = [\boldsymbol{c}\times]\bar{\boldsymbol{H}}_{0a}\bar{\boldsymbol{H}}_{aa}^{-1} = mc^2\boldsymbol{G}_{\omega a}\bar{\boldsymbol{H}}_{aa}^{-1} \tag{12}$$

The equation $\boldsymbol{\iota}_a = \bar{\boldsymbol{H}}_{aa}\Delta\dot{\boldsymbol{q}}_a$ can also be used to determine the impulse required at the actuators to achieve a given change in actuated joint velocity. This can be used to select which of a set of possible $\Delta\dot{\boldsymbol{q}}_a$ unit vectors would require the least energy to achieve, given the inertias of the links.

B. Spatial Method

Using spatial notation, the centroidal momentum of a system is defined as the aggregated angular and linear momenta of the system's links computed at the system's overall COM [3], [13]. The linear component ($\boldsymbol{l}$) of the centroidal momentum ($\hat{\boldsymbol{h}}_C$) is the linear momentum of the system ($\boldsymbol{l} = m\dot{\boldsymbol{c}}$), while the angular component ($\boldsymbol{k}_C$) is the total angular momentum the system has about its COM.

As shown in Equation (9), the momentum gains of a system are calculated using only its change in linear momentum, $\Delta\boldsymbol{l}$. This is due to angular momentum gain using the change in moment of momentum about the contact point.

The reason for using this change in moment of momentum is that the instantaneous change in total angular momentum about a passive rotary joint is always 0, and therefore using the above notation $\Delta\boldsymbol{k}_0 = \boldsymbol{0}_{3\times1}$. Therefore, using the contact point as a reference point, the change in angular momentum about the COM is: $\Delta\boldsymbol{k}_C = \Delta\boldsymbol{k}_0 - \boldsymbol{c}\times\Delta\boldsymbol{l} = -\boldsymbol{c}\times\Delta\boldsymbol{l}$.

This equation is included in the spatial transformation matrix ($\boldsymbol{X}_C$) from the contact point to the COM, which maps the total system momentum at the contact point to the centroidal momentum: $\hat{\boldsymbol{h}}_C = \boldsymbol{X}_C^T\hat{\boldsymbol{h}}_0$. Using $\boldsymbol{X}_C$, and the fact that $\Delta\boldsymbol{k}_0 = \boldsymbol{0}_{3\times1}$ due to the passive contact, we define a system's spatial gain as $\hat{\boldsymbol{G}}_h = \Delta\hat{\boldsymbol{h}}_C$:

$$\hat{\boldsymbol{G}}_h = \boldsymbol{X}_C^T\Delta\hat{\boldsymbol{h}}_0 = \begin{bmatrix}\boldsymbol{I}_{3\times3} & -[\boldsymbol{c}\times]\\ \boldsymbol{0}_{3\times3} & \boldsymbol{I}_{3\times3}\end{bmatrix}\begin{bmatrix}\boldsymbol{0}_{3\times1}\\ \Delta\boldsymbol{l}\end{bmatrix} = \begin{bmatrix}\boldsymbol{G}_k\\ \boldsymbol{G}_l\end{bmatrix} \tag{13}$$

where $\boldsymbol{G}_k = -\boldsymbol{c}\times\Delta\boldsymbol{l} = -mc^2\Delta\dot{\boldsymbol{\phi}}$ and $\boldsymbol{G}_l = \Delta\boldsymbol{l} = m\Delta\dot{\boldsymbol{c}}$.

If we assume that $||\Delta\dot{\boldsymbol{q}}_a|| = 1$, then we can define these gains in terms of the velocity gains:

$$\boldsymbol{G}_k(\Delta\dot{\boldsymbol{q}}_a) = -mc^2\boldsymbol{G}_\omega \quad \boldsymbol{G}_l(\Delta\dot{\boldsymbol{q}}_a) = m\begin{bmatrix}\boldsymbol{G}_v\\ G_g(\Delta\dot{\boldsymbol{q}}_a)\end{bmatrix} \tag{14}$$

while if we assume that $||\boldsymbol{\iota}_a|| = 1$, we can define them in terms of momentum gains:

$$\boldsymbol{G}_k(\boldsymbol{\iota}_a) = -\boldsymbol{G}_o \qquad \boldsymbol{G}_l(\boldsymbol{\iota}_a) = \begin{bmatrix}\boldsymbol{G}_m\\ G_g(\boldsymbol{\iota}_a)\end{bmatrix} \tag{15}$$

Notice that $\boldsymbol{G}_l$ includes a vertical component of linear gain, labeled G_g, which could be used as a measure of hopping ability (as discussed later in Section VI). This is similar to the component of $\boldsymbol{G}_\omega$ about a vertical axis, which could be used as a measure of spinning (as noted in [7]).

As with the previous gains, we can use these equations to define gain matrices for $\boldsymbol{G}_l(\Delta\dot{\boldsymbol{q}}_a)$ and $\boldsymbol{G}_k(\Delta\dot{\boldsymbol{q}}_a)$:

$$\boldsymbol{G}_{la}(\Delta\dot{\boldsymbol{q}}_a) = \bar{\boldsymbol{H}}_{0a} \qquad \boldsymbol{G}_{ka}(\Delta\dot{\boldsymbol{q}}_a) = -[\boldsymbol{c}\times]\bar{\boldsymbol{H}}_{0a} \tag{16}$$

For the momentum equivalents, we post-multiply these gain matrices by $\bar{\boldsymbol{H}}_{aa}^{-1}$ to get $\boldsymbol{G}_{la}(\boldsymbol{\iota}_a) = \boldsymbol{G}_{la}(\Delta\dot{\boldsymbol{q}}_a)\bar{\boldsymbol{H}}_{aa}^{-1}$ and $\boldsymbol{G}_{ka}(\boldsymbol{\iota}_a) = \boldsymbol{G}_{ka}(\Delta\dot{\boldsymbol{q}}_a)\bar{\boldsymbol{H}}_{aa}^{-1}$. Combining these, we can also define the gain matrix $\boldsymbol{G}_{ha}(\Delta\dot{\boldsymbol{q}}_a)$ in terms of $\bar{\boldsymbol{H}}_{0a}$ (and as before, $\boldsymbol{G}_{ha}(\boldsymbol{\iota}_a) = \boldsymbol{G}_{ha}(\Delta\dot{\boldsymbol{q}}_a)\bar{\boldsymbol{H}}_{aa}^{-1}$):

$$\hat{\boldsymbol{G}}_h(\Delta\dot{\boldsymbol{q}}_a) = \begin{bmatrix}-[\boldsymbol{c}\times]\\ \boldsymbol{I}_{3\times3}\end{bmatrix}\bar{\boldsymbol{H}}_{0a}\Delta\dot{\boldsymbol{q}}_a = \boldsymbol{G}_{ha}(\Delta\dot{\boldsymbol{q}}_a)\Delta\dot{\boldsymbol{q}}_a \tag{17}$$

The centroidal momentum matrix $\boldsymbol{A}_C$ relates the centroidal momentum of a system to its joint velocities: $\hat{\boldsymbol{h}}_C = \boldsymbol{A}_C\dot{\boldsymbol{q}}$ [3], [13]. If we divide $\boldsymbol{A}_C$ into passive and actuated elements ($\boldsymbol{A}_C = [\boldsymbol{A}_{Cp}\ \boldsymbol{A}_{Ca}]$), then we can define an actuated centroidal momentum matrix $\bar{\boldsymbol{A}}_{Ca}$ as:

$$\begin{aligned}\Delta\hat{\boldsymbol{h}}_C &= \boldsymbol{A}_{Cp}\Delta\dot{\boldsymbol{q}}_p + \boldsymbol{A}_{Ca}\Delta\dot{\boldsymbol{q}}_a\\ &= (\boldsymbol{A}_{Ca} - \boldsymbol{A}_{Cp}\boldsymbol{H}_{pp}^{-1}\boldsymbol{H}_{pa})\Delta\dot{\boldsymbol{q}}_a\\ &= \bar{\boldsymbol{A}}_{Ca}\Delta\dot{\boldsymbol{q}}_a\end{aligned} \tag{18}$$

Using this definition, and our definition of spatial gain as $\hat{\boldsymbol{G}}_h = \Delta\hat{\boldsymbol{h}}_C$, we can show that $\bar{\boldsymbol{A}}_{Ca} = \boldsymbol{G}_{ha}(\Delta\dot{\boldsymbol{q}}_a)$, since

$$\boldsymbol{G}_{ha}\Delta\dot{\boldsymbol{q}}_a = \hat{\boldsymbol{G}}_h = \Delta\hat{\boldsymbol{h}}_C = \boldsymbol{A}_C\Delta\dot{\boldsymbol{q}} = \bar{\boldsymbol{A}}_{Ca}\Delta\dot{\boldsymbol{q}}_a \tag{19}$$

These definitions provide us with an alternative method of calculating both the velocity and momentum gains of a system using the well known centroidal momentum equations. They also provide an intuitive interpretation for control algorithms based on centroidal momentum [2]–[4].

Velocity and momentum gains quantify the fundamental physical limits of a system's COM motion, and by extension its ability to balance. As demonstrated in [8]–[10], using the velocity gain directly in the system model enables excellent balance performance with even a simple PID controller.

Based on the inherent relationship between the centroidal momentum and these gains, which led to our definition of the spatial gain, more complex controllers which use centroidal momentum to balance should also demonstrate excellent balance performance. While using the gains (either directly or indirectly) as part of a control strategy can lead to balance performance near the peak of what a given system is capable of, they can also be used to optimize a system's physical properties to maximize its peak balance performance.

IV. Optimization-Based Mechanism Design

We illustrate the benefit of using the momentum gains for designing parameterized mechanisms, described in more detail in [14]. The optimization framework we have developed requires five main elements to be defined:

- A model, defining the parameterized mechanism (including the number of links, joint details, etc.);
- A set of key poses $\boldsymbol{Q} = \{\boldsymbol{q}_1, \boldsymbol{q}_2, \dots\}$ for the model's joints (including the passive joint);
- The modifiable parameters $\boldsymbol{x}$ of the model (e.g., mass, length, link COM), with their allowable upper and lower bounds ($\boldsymbol{x}_{min}$ and $\boldsymbol{x}_{max}$, can be $\pm\infty$ if desired);
- A parameter map, which dictates how to assign a given set of parameters $\boldsymbol{x}$ to the model; and
- An overall objective function $J(\boldsymbol{x})$ which quantifies the mechanism's desired behavior for a given $\boldsymbol{x}$.

Once these five elements have been selected, a global optimization is used to find the "best" parameterization:

$$\max_{\boldsymbol{x}} J(\boldsymbol{x}), \quad \text{s.t.} \quad \boldsymbol{x}_{min} \leq \boldsymbol{x} \leq \boldsymbol{x}_{max} \tag{20}$$

The objective function in this work is the mean pose-specific objective function $J(\boldsymbol{q}, \boldsymbol{x})$ across all n_q key poses:

$$J(\boldsymbol{x}) = \frac{1}{n_q} \sum_{\boldsymbol{q}} J(\boldsymbol{q}, \boldsymbol{x}) \qquad \forall \boldsymbol{q} \in \boldsymbol{Q} \tag{21}$$

Four pose-specific objective functions have been defined using the magnitudes of the velocity and momentum gains to quantify the model's balancing ability (where the dependence on $\boldsymbol{q}$ and $\boldsymbol{x}$ is implicit as part of the gain definitions):

$$\begin{aligned} J_v(\boldsymbol{q}, \boldsymbol{x}) &= \max_{\Delta\dot{\boldsymbol{q}}_a} |\boldsymbol{G}_v(\Delta\dot{\boldsymbol{q}}_a)| \quad \text{s.t. } ||\Delta\dot{\boldsymbol{q}}_a|| = 1 \\ J_\omega(\boldsymbol{q}, \boldsymbol{x}) &= \max_{\Delta\dot{\boldsymbol{q}}_a} |\boldsymbol{G}_\omega(\Delta\dot{\boldsymbol{q}}_a)| \quad \text{s.t. } ||\Delta\dot{\boldsymbol{q}}_a|| = 1 \\ J_m(\boldsymbol{q}, \boldsymbol{x}) &= \max_{\boldsymbol{\iota}_a} |\boldsymbol{G}_m(\boldsymbol{\iota}_a)| \quad \text{s.t. } ||\boldsymbol{\iota}_a|| = 1 \\ J_o(\boldsymbol{q}, \boldsymbol{x}) &= \max_{\boldsymbol{\iota}_a} |\boldsymbol{G}_o(\boldsymbol{\iota}_a)| \quad \text{s.t. } ||\boldsymbol{\iota}_a|| = 1 \end{aligned} \tag{22}$$

Note that although $\boldsymbol{q}$ and $\boldsymbol{x}$ are fixed, the $\Delta\dot{\boldsymbol{q}}_a$ or $\boldsymbol{\iota}_a$ unit vector which maximizes the velocity or momentum gain, respectively, must be determined for each pair of $\boldsymbol{q}$ and $\boldsymbol{x}$.

By maximizing the mean of these objectives across all key poses as the overall objective and using the magnitude of the gains, any parameter set with zero crossings (or gains near zero) in the configuration set $\boldsymbol{Q}$ will be avoided.

The selected key poses in $\boldsymbol{Q}$ may cover a model's entire (active and passive) configuration space, if it is expected to regularly operate throughout the entire space, or can be used selectively to focus the optimization on a particular subset of the space (e.g., a biped standing on one or both feet).

A. Planar Objective Functions

A typical goal would be to find a unit velocity or impulse vector which maximizes a given gain for one configuration $\boldsymbol{q}$ of the model. The gain vectors are a useful tool for finding the $\Delta\dot{\boldsymbol{q}}_a$ or $\boldsymbol{\iota}_a$ vector which achieves this maximization.

For the purposes of balancing in the plane, the pose-specific objective functions can be simplified as follows:

- For velocity gains, the objective function is the norm of the gain vector, either linear or angular. Since velocity gains require $||\Delta\dot{\boldsymbol{q}}_a|| = 1$, these vector norms maximize the selected velocity gain for the given $(\boldsymbol{q}, \boldsymbol{x})$ pair.

$$\begin{aligned} J_v(\boldsymbol{q}, \boldsymbol{x}) &= \max_{\Delta\dot{\boldsymbol{q}}_a} |\boldsymbol{G}_v(\Delta\dot{\boldsymbol{q}}_a)| = ||\boldsymbol{G}_{va}(\boldsymbol{q}, \boldsymbol{x})|| \\ J_\omega(\boldsymbol{q}, \boldsymbol{x}) &= \max_{\Delta\dot{\boldsymbol{q}}_a} |\boldsymbol{G}_\omega(\Delta\dot{\boldsymbol{q}}_a)| = ||\boldsymbol{G}_{\omega a}(\boldsymbol{q}, \boldsymbol{x})|| \end{aligned} \tag{23}$$

- For momentum gains, the velocity gain vectors are replaced with momentum gain vectors, and the assumption is $||\boldsymbol{\iota}_a|| = 1$. As above, the objective function is the norm of the gain vector, which maximizes the selected momentum gain for the given $(\boldsymbol{q}, \boldsymbol{x})$ pair.

$$\begin{aligned} J_m(\boldsymbol{q}, \boldsymbol{x}) &= \max_{\boldsymbol{\iota}_a} |\boldsymbol{G}_m(\boldsymbol{\iota}_a)| = ||\boldsymbol{G}_{ma}(\boldsymbol{q}, \boldsymbol{x})|| \\ J_o(\boldsymbol{q}, \boldsymbol{x}) &= \max_{\boldsymbol{\iota}_a} |\boldsymbol{G}_o(\boldsymbol{\iota}_a)| = ||\boldsymbol{G}_{oa}(\boldsymbol{q}, \boldsymbol{x})|| \end{aligned} \tag{24}$$

Note that the objective functions depend on the norm used to define the unit vectors $||\Delta\dot{\boldsymbol{q}}|| = 1$ and $||\boldsymbol{\iota}_a|| = 1$: If the 1-norm is used to define the unit vector, then the objective functions use the ∞-norm. Similarly, if the ∞-norm is used to define the unit vector, then the objective functions use the 1-norm. Finally, if the 2-norm is used to define the unit vector, the objective functions will also use the 2-norm. See the Appendix for details on these norm relationships.

V. Planar Examples

Using the objective functions and optimization framework described in the previous section, three example models were selected to help demonstrate the benefits of using momentum gain as the design criterion (with n_i the number of independent links and n_a the number of actuated joints):

- A 2-link inverted pendulum, ($n_i = 2$, $n_a = 1$)
- A 3-link biped, and ($n_i = 2$, $n_a = 2$)
- A 3-link inverted pendulum. ($n_i = 3$, $n_a = 2$)

Note that in the biped model the legs are assumed to be identical, so only one of the legs is independently parameterized. Three parameters are used for each independent link:

- The fraction of total mass in each link, $0 < m_i/m < 1$;
- The position of the link's COM along the link (as a fraction of its length), $0 < c_i/l_i \leq 1$; and
- The length of the link, $0 < l_i \leq 1$.

Unless otherwise noted, the elements of $\boldsymbol{x}_{min}$ are all set to a small positive value $\epsilon > 0$, to ensure that the link masses, COMs, and lengths remain within a reasonable range for an actual mechanism. Since the gains are invariant to a scaling of the total mass, we assume $m = \sum_i m_i = 1$ (reducing the number of independent parameters by 1 for every model).

For each of the example models, an optimization was run for each objective function. To generate specific key poses to populate $\boldsymbol{Q}$, ranges were set for each joint (passive and active) as shown in Table I and key poses were automatically generated to uniformly span the desired joint space.

TABLE I

JOINT RANGES USED TO GENERATE KEY POSES.

Joint Types	**Passive**	**Actuated**	
Model	$\boldsymbol{q_1}$	$\boldsymbol{q_2}$	$\boldsymbol{q_3}$
2-Link IP	$\pm\pi/4$	$\pm\pi/2$	
3-Link Biped	$\pm\pi/4$	$\pm\pi/2$	$\pm\pi/2$
3-Link IP	$\pm\pi/4$	$\pm\pi/2$	$\pm\pi/2$

The joint ranges shown in Table I have been selected to maximize the number of key poses which are likely to be encountered by a real-world mechanism with the given form. With this in mind, the body angle specified for the biped model is relative to a vertical axis to mimic the typically upright bodies of bipeds. Similarly, the biped's swing leg hip joint has been flipped so that an angle of 0 points down instead of up, as is typical in biped robots.

A. 2-Link Inverted Pendulum

For this model, both links were parameterized as discussed above, leading to a total of 6 parameters. Since the length of the final link (furthest from the contact point) has no effect on the gains, we assume $c_2/l_2 = 1$. This change, in combination with setting $m = 1$, leaves 4 independent parameters.

Although it has been suggested that analysis of a planar 2-link inverted pendulum with only 1 actuated joint does not benefit from using momentum gain over velocity gain [7], in the case of mechanism design there is a benefit to using momentum rather than velocity gains. Since the lengths, masses, and link COMs are free to change in this formulation, the momentum gain includes additional useful information about the mechanism's ability to balance which is not available if the velocity gain is used.

This is demonstrated in Table II and the diagrams in Figure 2a, where the results of running the four different optimizations are summarized. Each optimization has successfully found a parameter set which maximizes the desired gain, but the best solution found differs greatly for each gain.

TABLE II

PARAMETER SETS FOR 2-LINK INVERTED PENDULUM

2-Link IP	$\frac{\boldsymbol{m_1}}{\boldsymbol{m}}$	$\frac{\boldsymbol{c_1}}{\boldsymbol{l_1}}$	$\boldsymbol{l_1}$	$\frac{\boldsymbol{m_2}}{\boldsymbol{m}}$	$\frac{\boldsymbol{c_2}}{\boldsymbol{l_2}}$	$\boldsymbol{l_2}$
Optim. for $\boldsymbol{G}_v$	.1	1	1	.9	1	1
Optim. for $\boldsymbol{G}_\omega$	.9	1	.134	.1	1	.831
Optim. for $\boldsymbol{G}_m$	.9	.1	.1	.1	1	.1
Optim. for $\boldsymbol{G}_o$	.1	.1	.1	.9	1	1

TABLE III

PARAMETER SETS FOR 3-LINK BIPED

3-Link Biped	$\frac{\boldsymbol{m_1}}{\boldsymbol{m}}$	$\frac{\boldsymbol{c_1}}{\boldsymbol{l_1}}$	$\boldsymbol{l_1}$	$\frac{\boldsymbol{m_2}}{\boldsymbol{m}}$	$\frac{\boldsymbol{c_2}}{\boldsymbol{l_2}}$	$\boldsymbol{l_2}$
Optim. for $\boldsymbol{G}_v$	.45	.1	1	.1	1	1
Optim. for $\boldsymbol{G}_\omega$	.45	.1	.232	.1	1	.719
Opttim. for $\boldsymbol{G}_m$	.1	.9	.1	.8	1	.1
Optim. for $\boldsymbol{G}_o$	.1	.9	.1	.8	1	1

TABLE IV

PARAMETER SETS FOR 3-LINK INVERTED PENDULUM [4]

3-Link IP	$\frac{\boldsymbol{m_1}}{\boldsymbol{m}}$	$\frac{\boldsymbol{c_1}}{\boldsymbol{l_1}}$	$\boldsymbol{l_1}$	$\frac{\boldsymbol{m_2}}{\boldsymbol{m}}$	$\frac{\boldsymbol{c_2}}{\boldsymbol{l_2}}$	$\boldsymbol{l_2}$	$\frac{\boldsymbol{m_3}}{\boldsymbol{m}}$	$\frac{\boldsymbol{c_3}}{\boldsymbol{l_3}}$	$\boldsymbol{l_3}$
Optim. for $\boldsymbol{G}_v$	.1	1	1	.1	.1	1	.8	1	1
Feath. Init. [7]	.333	1	.3	.333	1	.3	.333	1	.3
Feath. Impr. [7]	.467	1	.2	.333	1	.25	.2	1	.35
Optim. for $\boldsymbol{G}_\omega$	.8	1	.115	.1	.1	.1	.1	1	1
Optim. for $\boldsymbol{G}_m$	.8	.1	.1	.1	.1	.1	.1	1	.1
Optim. for $\boldsymbol{G}_o$	.1	.1	1	.1	.1	.1	.8	1	1

B. 3-Link Biped

For this model, 2 of the 3 links were parameterized as discussed above, leading to a total of 6 parameters. The third link is defined as an identical copy of the first link.

Due to the symmetry created by using identical legs, the upper bounds in $\boldsymbol{x}_{max}$ were set to $1-\epsilon$ for the leg link COMs and remained set to 1 for all other parameters. Since the length of the body link has no effect on the gain calculations (much like the final link in inverted pendulums) we again assume $c_2/l_2 = 1$, which leaves 4 independent parameters.

Table III summarizes the results of the 4 different optimizations using our framework for the 3-link biped model, with associated diagrams shown in Figure 2b.

C. 3-Link Inverted Pendulum

For this model, each of the 3 links was parameterized as discussed above, leading to a total of 9 parameters. As before, we set $m = 1$ and the COM of the final link at the end of the link ($c_3/l_3 = 1$), which leaves 7 independent parameters.

This type of model was used as a design example by Featherstone in [7] where the center of mass of each of the links was fixed to the end of the link (i.e., $c_i/l_i = 1$), leaving

[4]Although $m = 1.5$ for both of Featherstone's models, the mass fractions are used in Table IV and the gain calculations. Only the relative mass matters, since all of the gains are invariant to a scaling of the mass.

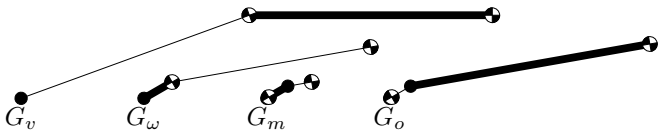

(a) 2-Link Inverted Pendulum Models from Table II

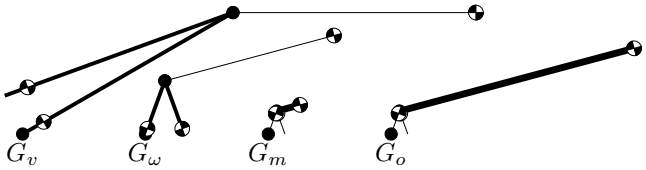

(b) 3-Link Biped Models from Table III

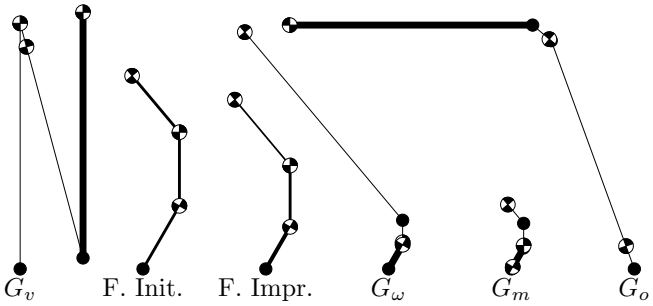

(c) 3-Link Inverted Pendulum Models from Table IV

Fig. 2. Diagrams of the three different example models which correspond to the optimization results in Tables II, III, and IV. In these diagrams, the relative thicknesses of each link denote their relative masses. Note that the configurations of the models' joint angles in these figures are arbitrary.

6 independent parameters which were initialized to $m_i = .5$ and $l_i = .3$. They then manually explored the parameter space and compared angular velocity gain plots to determine how to improve on their initial design.

Table IV and the diagrams in Figure 2c include the two parameterizations from [7], as well as the results of the 4 different optimizations using our framework. It should be noted that although $m = 1.5$ for the original Featherstone models, the mass fractions are used in the table and gain calculations as it is only the relative mass which matters since the gains are invariant to a scaling of the mass.

D. Observations for Inverted Pendulums

For $\boldsymbol{G}_v$, placing maximum mass as far from the contact point as possible maximizes every joint's potential ability to move the COM. We also expect the links to be as long as possible, since $\boldsymbol{G}_v$ has units of length.

For $\boldsymbol{G}_\omega$, we expect to see the COM as close to the first joint as possible while maintaining the ability to rotate the COM around the contact point by placing a small mass far away. This is due to the invariance of $\boldsymbol{G}_\omega$ to changes in q_1 for a point contact (which shifts the desired COM from the contact point to the first joint) and that $\boldsymbol{G}_\omega \propto 1/c$.

Both momentum gains include their corresponding velocity gains, but the inertial loading on the joints is now included via multiplication by $\bar{\boldsymbol{H}}_{aa}^{-1}$, which in the 2-link IP case reduces to $\bar{H}_{22}^{-1} = H_{11}/det(\boldsymbol{H}) = \Delta\dot{q}_2/\iota_2$.

This effectively makes it expensive to move mass which is far from the actuated joints by penalizing high joint torques. This is qualitatively different from penalizing high joint accelerations, as is the case with velocity gains.

We see the effects of this on the $\boldsymbol{G}_m$ IP examples, with the majority of the mass very close to the contact point. We also see very short links, as $\boldsymbol{G}_m$ has units of reciprocal length.

Considering the $\boldsymbol{G}_o$ IP results, we can see the influence of the additional c^2 term which causes $\boldsymbol{G}_o \propto c$: the majority of the mass is placed far away from the contact. The remainder of the mass is then placed so as to minimize the required torque demands for balancing (close to the contact for IPs).

E. Observations for 3-Link Biped

For $\boldsymbol{G}_v$, the biped's mass has moved to its feet instead of keeping it far from the contact. This is mainly a function of the selected key poses maintaining the body link above and the feet below the hips, such that a smaller mass in the leg contributes more to the horizontal COM motion for a given joint velocity than a larger body mass.

Effectively, due to the passive joint at the contact enforcing conservation of angular momentum about the contact, moving a moderate-sized mass close to the contact requires a smaller passive rotation to compensate, and therefore a larger overall horizontal motion of the COM.

These heavy legs are also due to there being no consideration of the inertial loading or location of the COM in the $\boldsymbol{G}_v$ equations, only a ratio between horizontal COM velocity and joint velocity. The biped which is optimized for $\boldsymbol{G}_\omega$ also has heavy feet, due to the same effect.

We see the analog of the momentum gain IP effects in the biped, where locating most of the mass in the body and placing the COMs of the legs close to the hips means it is very cheap to move the swing leg. This is the direct opposite of what we saw for the velocity gains, where there is no cost to swing a heavy leg. For $\boldsymbol{G}_o$, this serves to minimize the required torque demands for balancing (as done in the IPs).

F. Comparison between Gains

Based on the results above, as well as comparing the formulations of the velocity and momentum gains, several key differences become apparent. These observable differences exist not only between velocity and momentum gains, but also between the linear and angular gains of the same type.

The inclusion of inertial effects in the momentum gains compared to the velocity gains enables them to act as a proxy for energy efficiency. Since momentum gains incorporate a consideration of the amount of joint impulse required to move the COM relative to the contact point, maximizing the momentum gain for a given configuration has the same effect as minimizing the joint torques. Maximizing velocity gains will only provide a proxy for minimizing joint accelerations for a given configuration, which is not equivalent.

Comparing the linear and angular gains of each type, the angular gains are more suitable for mechanism design as they are dimensionless and, when the contact can be approximated as a spherical (rotary in 2D) joint, invariant to the passive contact angle(s). Both these properties reduce the complexity of the design space, while maintaining the means to quantify

the physical ability of a mechanism to move its COM relative to the contact. Using dimensionless metrics removes the dependence on scale from the calculation, allowing angular velocity and momentum gains to be used across a family of different mechanisms at various masses and lengths.

Looking specifically at the biped results in Table III and Figure 2b, it is apparent that designing a biped using velocity gains will produce an inefficient walking mechanism due to the heavy feet. Compare this to the designs based on momentum gain, which place most of their mass in the body and shift the leg masses as close to the hip as possible to minimize hip torques. Due to the above issues with the linear gains and velocity gains, the preferred gain for mechanism design (at least in the case of a planar biped) is the angular momentum gain, which was used in [14] for this purpose.

VI. Discussion

Since the linear velocity and momentum gains have units of length and reciprocal length, respectively, they are dependent on not just the relative lengths of the links but the total length (height for biped) of the system. This is directly evident in the examples in the previous section, where all of the links had the maximum length when optimizing for G_v and minimum length when optimizing for G_m.

In light of this, for a real world scenario there would need to be either more restrictive limits set on the lengths for the links (or fixed lengths, if appropriate) or a fixed overall length (or height) which can then be used to parameterize using a ratio of link length to total length.

We also considered whether other forms of overall objective function would change the results or achieve higher gains across more key poses, such as using the median or minimum of the gains over all poses. For example, when using the minimum of the gains, the value of the objective function represents the guaranteed worst case gain for the system across all poses. A critical consideration when using the mean is that it can be more sensitive to the set of key poses used to define the joint ranges than other options.

The main existing application of velocity gains are the planar momentum-based controllers in [8]–[10]. The plant model gains in [10] can be defined using $\bar{\boldsymbol{H}}$ notation as:

$$Y_1 = \frac{-H_{x1}}{H_{11}\bar{H}_{x2}} \qquad Y_2 = \frac{-1}{g\bar{H}_{x2}} \qquad \boldsymbol{Y}_3 = \frac{\bar{\boldsymbol{H}}_{x3}}{\bar{H}_{x2}} \tag{25}$$

Comparing the common element $\bar{H}_{x2} = mG_v$ to Equation (16), the model defined in [10] could equivalently use the horizontal component of $G_l(\Delta\dot{\boldsymbol{q}}_a)$. Similarly, a majority of recent work on whole body balance uses centroidal momentum (e.g., [2]–[4]), which also use controllers which could be defined using spatial gain. An examination of the relationship between balancing a system using centroidal momentum and the evolution of its spatial gain is warranted.

As mentioned in [7], the angular gains in 3D include a vertical component, which does not contribute to balance but to spinning around the contact point. The linear analog are the vertical gains defined in this work as G_g, which also do not contribute to balance. However, they could be used as a method of quantifying the capability of a system to move vertically, with applications in hopping or bouncing.

The momentum gains defined in this paper can be easily extended to the case of rolling contact, knife-edge contact, or a compliant base of support in 2D or 3D, similar to how the velocity gains have been extended in [7]. However, assuming the system has only a single contact with the environment (or mimics one via compliance) is the main limitation of both velocity and momentum gains.

This can be partially overcome by assuming a set of one or more co-located joints, such as at an ankle or hip, is passive. This set of joints can then be used in place of the contact point, allowing the momentum and velocity gains to be applied. To determine the physical capabilities of a system with multiple contacts where a set of co-located joints cannot be assumed passive, a more complex metric is needed such as dynamic COM manipulability [6].

VII. Conclusion

In this work we have extended Featherstone's initial definition of momentum gain for planar 2-link inverted pendulums to general 2D and 3D mechanisms, along with defining new notation to simplify both the velocity and momentum gain equations. We have also described two different methods for calculating these general momentum gains, namely the Augmented Inertia method and the Spatial method.

The Spatial method development also provides insight on the relationship between a system's centroidal momentum and its velocity and momentum gains. This enabled us to define the spatial gain of a system, incorporating both angular and linear components in all 6 directions of 3D motion, and to define an actuated centroidal momentum matrix which we showed to be equivalent to the spatial gain matrix.

One direction for future work resulting from this research is the use of the velocity and momentum gains in parallel with other suitable objectives for the design of a more complex system. This would benefit from an examination of the *position gains*, defined briefly in [7] as the integral of velocity gain along a path in configuration space, and the analogous gains found by integrating the momentum gains along a similar configuration space path.

Appendix

In the planar case, the pose-specific objective functions make use of vector norms to simplify their calculations. The vector norm to use will depend on the norm being used to determine the magnitude of the unit vector in question. In general, assuming a unit vector $\boldsymbol{u}_a$, gain $G(\boldsymbol{u}_a)$, and gain vector $\boldsymbol{G}_a$, we can define the following:

$$\begin{aligned} J(\boldsymbol{q},\boldsymbol{x}) &= \max_{\boldsymbol{u}_a} |G(\boldsymbol{u}_a)| && \text{s.t. } ||\boldsymbol{u}_a|| = 1 \\ &= \max_{\boldsymbol{u}_a} |\boldsymbol{G}_a\boldsymbol{u}_a| && \text{s.t. } ||\boldsymbol{u}_a|| = 1 \\ &= \max_{\boldsymbol{u}_a} |\textstyle\sum_{i\in a} G_i u_i| && \text{s.t. } ||\boldsymbol{u}_a|| = 1 \end{aligned} \tag{26}$$

Since we can freely choose $\boldsymbol{u}_a$ provided it satisfies $||\boldsymbol{u}_a|| = 1$, the magnitude brackets can be dropped by

matching the signs of G_i and u_i (i.e., $\forall i \in a, G_i u_i \geq 0$):

$$J(\boldsymbol{q}, \boldsymbol{x}) = \max_{\boldsymbol{u}_a} \textstyle\sum_{i \in a} G_i u_i \quad \text{s.t.} ||\boldsymbol{u}_a|| = 1 \tag{27}$$

If the ∞-norm is used to determine the magnitude of the unit vector ($||\boldsymbol{u}_a||_\infty = \max_{i \in a} |u_i| = 1$), the maximum magnitude of the gain will occur when $\forall i \in a, |u_i| = 1$. Similarly, if the 1-norm is used to determine the magnitude of the unit vector ($||\boldsymbol{u}_a||_1 = \sum_{i \in a} |u_i| = 1$), the maximum magnitude of the gain will occur when $|u_j| = 1$ and $\forall k \in a \neq j, u_k = 0$ (where j is the index of the largest magnitude element in $\boldsymbol{G}_a$). This leads to the following simplifications:

$$\begin{aligned} J(\boldsymbol{q}, \boldsymbol{x}) &= ||\boldsymbol{G}_a||_\infty \qquad \text{if } ||\boldsymbol{u}_a||_1 = 1 \\ J(\boldsymbol{q}, \boldsymbol{x}) &= ||\boldsymbol{G}_a||_1 \qquad \text{if } ||\boldsymbol{u}_a||_\infty = 1 \end{aligned} \tag{28}$$

Finally, if the 2-norm is used to determine the magnitude of the unit vector ($||\boldsymbol{u}_a||_2 = \sqrt{\sum_{i \in a} u_i^2} = 1$), the following simplification can be used based on the definition of the inner product as $\boldsymbol{a} \cdot \boldsymbol{b} = ||\boldsymbol{a}||_2 \ ||\boldsymbol{b}||_2 \cos\theta$ (where θ is the angle between the vectors):

$$\begin{aligned} J(\boldsymbol{q}, \boldsymbol{x}) &= \max_{\boldsymbol{u}_a} |\boldsymbol{G}_a \boldsymbol{u}_a| \qquad && \text{s.t. } ||\boldsymbol{u}_a||_2 = 1 \\ &= \max_{\boldsymbol{u}_a} |\boldsymbol{G}_a^T \cdot \boldsymbol{u}_a| \qquad && \text{s.t. } ||\boldsymbol{u}_a||_2 = 1 \\ &= \max_{\boldsymbol{u}_a} ||\boldsymbol{G}_a^T||_2 \ |\cos\theta| \qquad && \text{s.t. } ||\boldsymbol{u}_a||_2 = 1 \end{aligned} \tag{29}$$

Since $\boldsymbol{G}_a$ is a function only of $\boldsymbol{q}$ and $\boldsymbol{x}$, and we can freely choose $\boldsymbol{u}_a$ provided we maintain $||\boldsymbol{u}_a||_2 = 1$, we can force $|\cos\theta| = 1$ (its maximum value) by setting $\boldsymbol{u}_a$ parallel to $\boldsymbol{G}_a$. As their signs are equal, this means that to maximize the gain when $||\boldsymbol{u}_a||_2 = 1$ we set $\boldsymbol{u}_a = \boldsymbol{G}_a^T / ||\boldsymbol{G}_a^T||_2$.

Given that norms are independent of the orientation (row vs column) of the normed vector (i.e., $||\boldsymbol{G}_a|| = ||\boldsymbol{G}_a^T||$), this leads to the final simplification that is used in this paper:

$$J(\boldsymbol{q}, \boldsymbol{x}) = ||\boldsymbol{G}_a||_2 \qquad \text{if } ||\boldsymbol{u}_a||_2 = 1 \tag{30}$$

REFERENCES

[1] B. J. Stephens and C. G. Atkeson, "Dynamic Balance Force Control for Compliant Humanoid robots," in *IROS*, 2010, pp. 1248–1255.

[2] H. Dai, A. Valenzuela, and R. Tedrake, "Whole-body motion planning with centroidal dynamics and full kinematics," in *HUMANOIDS*, 2014, pp. 295–302.

[3] D. E. Orin, A. Goswami, and S.-H. Lee, "Centroidal dynamics of a humanoid robot," *Auton. Robots*, vol. 35, pp. 161–176, 2013.

[4] P. M. Wensing and D. E. Orin, "Improved Computation of the Humanoid Centroidal Dynamics and Application for Whole-Body Control," *Int. J. Humanoid Robot.*, vol. 13, no. 01, p. 1550039, 2016.

[5] F. L. Moro, "Balancing While Executing Competing Reaching Tasks: An Attractor-Based Whole-Body Motion Control System Using Gravitational Stiffness," *Int. J. Humanoid Robot.*, vol. 13, no. 01, p. 1550046, 2016.

[6] M. Azad, J. Babic, and M. Mistry, "Dynamic manipulability of the center of mass: A tool to study, analyse and measure physical ability of robots," in *ICRA*, 2017, pp. 3484–3490.

[7] R. Featherstone, "Quantitative measures of a robot's physical ability to balance," *Int. J. Rob. Res.*, vol. 35, no. 14, pp. 1681–1696, 2016.

[8] M. Azad, "Balancing and Hopping Motion Control Algorithms for an Under-actuated Robot," Ph.D. dissertation, Australian National University, 2014.

[9] M. Azad and R. Featherstone, "Angular momentum based balance controller for an under-actuated planar robot," *Auton. Robots*, vol. 40, no. 1, pp. 93–107, 2016.

[10] R. Featherstone, "A simple model of balancing in the plane and a simple preview balance controller," *Int. J. Rob. Res.*, pp. 1–19, 2017.

[11] R. Featherstone, *Rigid Body Dynamics Algorithms*, 2008.

[12] R. Featherstone and D. E. Orin, "Dynamics," in *Springer Handb. Robot.*, 2016, ch. 2, pp. 37–66.

[13] D. E. Orin and A. Goswami, "Centroidal Momentum Matrix of a humanoid robot: Structure and properties," in *IROS*, 2008, pp. 653–659.

[14] B. J. DeHart and D. Kulić, "Legged Mechanism Design with Momentum Gains," in *HUMANOIDS*, 2017.